Host–Guest Systems | Hot Paper

Deutsche Ausgabe: DOI: 10.1002/ange.201605676
Internationale Ausgabe: DOI: 10.1002/anie.201605676

Enhanced Electrochemical Kinetics on Conductive Polar Mediators for Lithium–Sulfur Batteries

*Hong-Jie Peng[+], Ge Zhang[+], Xiang Chen, Ze-Wen Zhang, Wen-Tao Xu, Jia-Qi Huang, and Qiang Zhang**

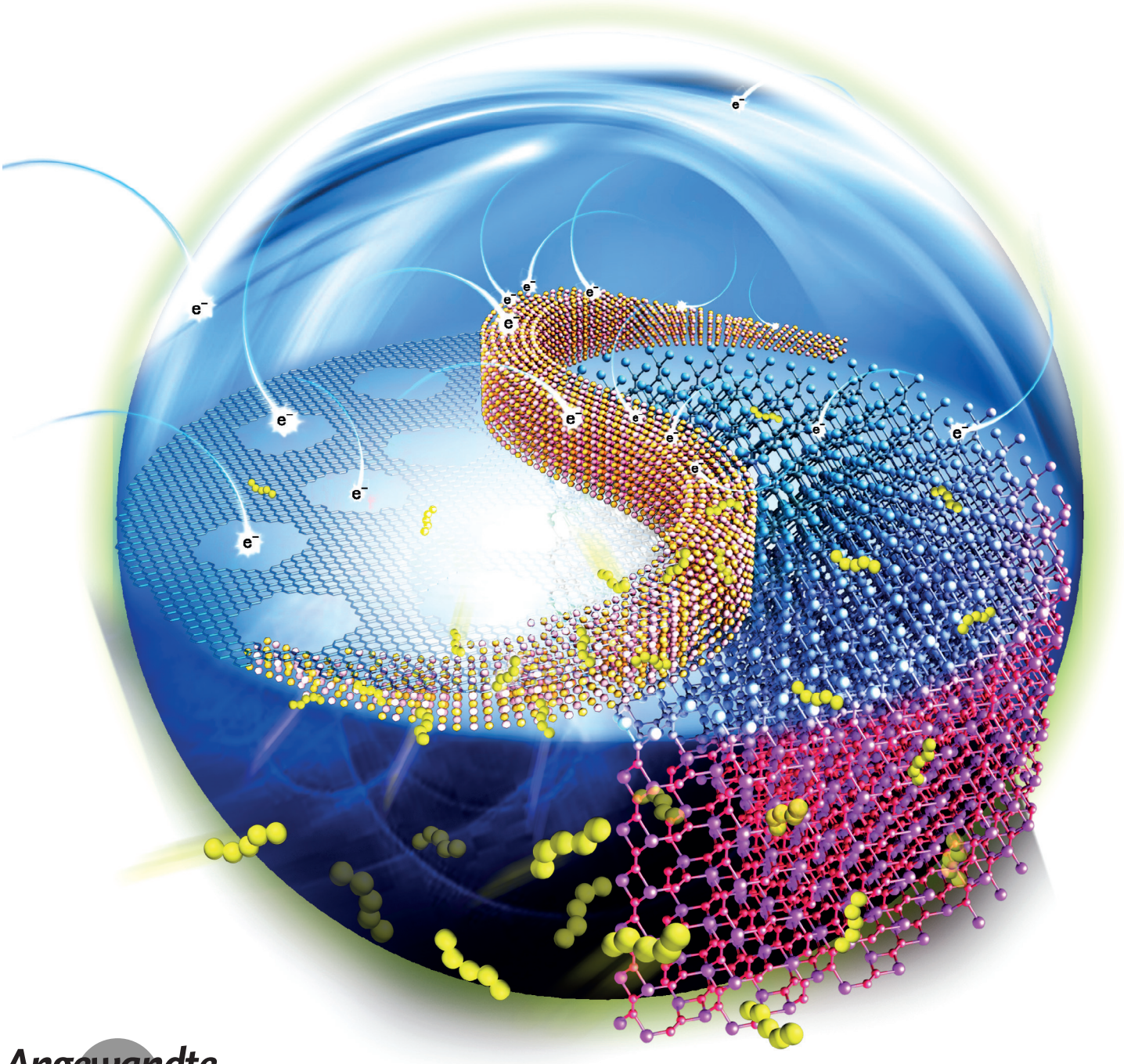

Abstract: *Lithium–sulfur (Li–S) batteries have been recognized as promising substitutes for current energy-storage technologies owing to their exceptional advantage in energy density. The main challenge in developing highly efficient and long-life Li–S batteries is simultaneously suppressing the shuttle effect and improving the redox kinetics. Polar host materials have desirable chemisorptive properties to localize the mobile polysulfide intermediates; however, the role of their electrical conductivity in the redox kinetics of subsequent electrochemical reactions is not fully understood. Conductive polar titanium carbides (TiC) are shown to increase the intrinsic activity towards liquid–liquid polysulfide interconversion and liquid–solid precipitation of lithium sulfides more than non-polar carbon and semiconducting titanium dioxides. The enhanced electrochemical kinetics on a polar conductor guided the design of novel hybrid host materials of TiC nanoparticles grown within a porous graphene framework (TiC@G). With a high sulfur loading of 3.5 mg cm^{-2}, the TiC@G/sulfur composite cathode exhibited a substantially enhanced electrochemical performance.*

To meet the growing demands for advanced energy storage technologies, lithium–sulfur (Li–S) batteries are recognized as promising substitutes for conventional lithium-ion batteries owing to their overwhelming energy density (2600 Wh kg^{-1}) as well as the natural abundance and environmental benignity of elemental sulfur.[1] Therefore, Li–S batteries have been gaining global attention over past few years. However, the complexity of the multi-electron redox reaction induces the shuttling of soluble polysulfides and drastic structural changes, which greatly impede the complete use of the sulfur in a Li–S cell.[2]

Tremendous efforts have been devoted to tailoring the nanostructure of carbon materials that serve as sulfur hosts to enhance their electrical conductivity and accommodate the active guest material.[3] However, the nonpolar nature of carbon makes carbon-based materials incapable of trapping polar polysulfides, which is the origin of the parasitic shuttle effect.[4] Moreover, the poor affinity of carbon for polysulfides also prevents the efficient interfacial charge transfer and slows down reaction kinetics.[5] Therefore, the mechanistic understanding and mediating of guest–host interactions to facilitate sulfur electrochemistry in aprotic electrolytes hold much promise for advancing the surface-chemistry-initiated design of novel polar host materials.

Heteroatom doping or co-doping was initially proposed to facilitate the chemisorption of sulfur-containing compounds onto carbon hosts.[6] However, the doping amount or the number of polar sites was very limited. Conductive polymers that contain nitrogen, oxygen, or sulfur heteroatoms are superb for the high doping level achieved compared to doped carbon.[7,8] However, it is challenging for a polymer to achieve an electrical or ionic conductivity comparable to that of carbon.

Most recently, polar inorganics were investigated to trap polysulfides or lithium sulfides. These materials share positive attributes, such as their superior reactivity and abundant surface sites, which enable a considerable reduction of the shuttle effect. However, their electrical conductivities vary significantly. Thus, they can be classified as conductors (for example, Magnéli-phase Ti_nO_{2n-1},[9] tin-doped indium oxide,[10] and MXene[11]), semimetals (for example, CoS_2[12] and TiS_2/VS_2[13]), semiconductors (for example, TiO_2,[14,15] MnO_2,[16,17] MoS_2,[18] and FeS_2[19]), and insulators (for example, SiO_2,[20] MgO,[21,22] and $Co(OH)_2$[23]). This diversity raises a fundamental issue of how the intrinsic conductivity of these polar materials affects the electrochemical kinetics of the Li–S redox. According to the reaction sequence, transformation of surface-bonded polysulfide moieties inevitably involves a charge transfer step. If the immobilizing surface is non-conductive, an additional surface diffusion step will be required for the overall reaction to proceed, as Tao et al. indicated.[22] The extra energy penalty that results from the surface diffusion further slows down the reaction kinetics. Therefore, it would be interesting and important to understand the role of conductivity in the electrochemical kinetics and to evaluate it at a relevant scale of other physical or structural parameters, which has been rarely the focus of previous reports.

Herein, these reaction kinetics were probed on the surfaces of congeneric titanium (Ti)-based inorganics with significantly different conductivities, namely semiconducting TiO_2 (10^{-10} S cm^{-1}) and metallic TiC (10^4 S cm^{-1}). Ti-based compounds have been extensively investigated owing to their low cost, environmental benignity, and desirable chemisorptivity towards polysulfides.[9,11,14] In contrast to previous reports, in which TiO_2 was compared with vacancy-rich conducting Ti_nO_{2n-1}, the influence of the surface density of uncoordinated sites was eliminated.[9] Loaded onto the surface of non-woven carbon-fiber paper (CP), bulk TiC particles exhibited a substantial improvement in both the reversible interfacial redox of polysulfides and the precipitation of lithium sulfides (Li_2S) compared to bare CP, whereas bulk TiO_2 particles did not. Incorporating the TiC nanoparticles into a mesoporous graphene framework through a confined carburization route resulted in a TiC@G hybrid host material with high surface area, large mesopore volume, and adequate interfacial affinity for a high-performance sulfur cathode. A high capacity of 1032 mAh g^{-1}, reversible and stable cycling over 100 cycles, and reduced polarization were obtained with a high sulfur loading of 3.5 mg cm^{-2}.

The interfacial electrochemical kinetics are dominated by two main factors (Figure 1 a). First, adequate binding affinity allows adsorption with sufficient surface coverage. Second, efficient charge transfer over the liquid–solid boundary facilitates the transport of the electrons generated during

[*] H.-J. Peng,[+] G. Zhang,[+] X. Chen, Z.-W. Zhang, W.-T. Xu, Prof. J.-Q. Huang, Prof. Q. Zhang
Beijing Key Laboratory of Green Chemical Reaction Engineering and Technology, Department of Chemical Engineering
Tsinghua University
Beijing 100084 (P.R. China)
E-mail: zhang-qiang@mails.tsinghua.edu.cn

[+] These authors contributed equally to this work.

Supporting information for this article can be found under: http://dx.doi.org/10.1002/anie.201605676.

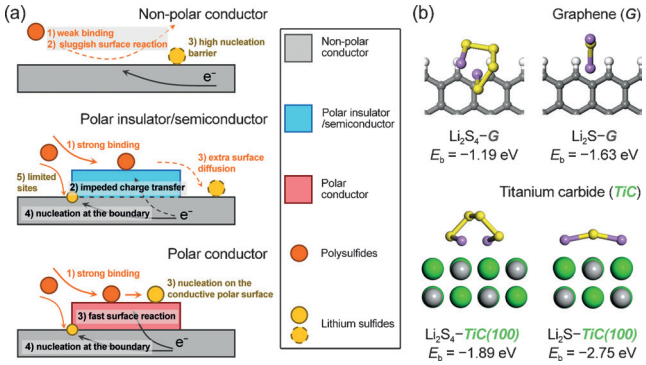

Figure 1. Role of polar conductor in surface reaction and nucleation. a) Illustration of the working mechanism of the polar conductor as it meets the demand for both adequate binding and charge transfer. b) First-principle calculations suggesting the higher binding energies of TiC to polysulfides (Li_2S_4) and Li_2S compared to pristine graphene.

the redox of the adsorbates. A non-polar host such as carbon is too inert to bind polar species, resulting in low coverage of reactive intermediates. Additionally, the difference in the surface energy between the host and deposited Li_2S nuclei increases the nucleation barrier. A polar insulator or semiconductor such as TiO_2 possesses the desirable chemical affinity necessary for enrichment of the surface-bonded species. However, its poor electrical conductivity impedes the direct surface conversion on the polar host. An additional surface diffusion step is required, otherwise nucleation can only occur at the ternary interface of the electrolyte, insulating host, and conductive substrate, in which the surface site density is inevitably low. Therefore, only a polar conductor can fully meet the demands for both sufficient surface binding and efficient charge transport. On such materials, the surface reaction and subsequent precipitation of solid products can proceed over the relatively abundant surface sites, which results in enhanced electrochemical kinetics.

The effectiveness of TiO_2 as a chemisorptive material for polysulfides has been demonstrated both experimentally and theoretically in the previous reports.[24] Ti_xC_y-type MXene has also been explored as a sulfur host, on which the highly reactive surface −OH groups were regarded as the main origin of chemisorption.[11] However, TiC with different stoichiometries and a clean surface has never been used in Li–S batteries. First-principle calculations were therefore conducted to reveal the interaction between TiC and the polar sulfur species. The binding energies (E_b) of Li_2S_4 and Li_2S to the TiC(100) surface are −1.89 and −2.75 eV, respectively, which were significantly higher than those on the graphene plane (Figure 1b). Static-adsorption results also show the enhanced adsorption of polysulfides by TiC powders (Supporting Information, Figure S1).

Polar inorganic compounds are commonly employed in Li–S batteries to retard the shuttling of polysulfides by strong chemical adsorption. However, their impact on electrochemical kinetics and the correlation to the electrical conductivity have not been fully understood. Therefore, kinetic studies of two probe reactions, polysulfide redox in the liquid phase and Li_2S precipitation, were conducted on CP and CP-supported TiO_2/TiC (denoted as CP-TiO_2/TiC) electrodes.

As demonstrated previously using symmetric cells, the low capacity and large polarization stem from the sluggish liquid–liquid redox of polysulfides.[12] Analogous symmetric cells composed of Li_2S_6 electrolyte between two identical electrodes were assembled. Electrochemical impedance spectra (EIS) of the symmetric cells indicated that CP-TiC exhibited a decrease of 70% in resistance compared to pristine CP (Figure 2a). Due to the advantageous lithium-free feature of the symmetric cells, such a decrease is attributed to the enhanced interfacial affinity between TiC and polysulfides. In contrast, the impedance of the CP-TiO_2 cell was still comparable to or even greater than that of CP, implying that a strong chemical interaction is not the only reason for enhanced kinetics. The conductivity should also strongly influence the interfacial transformation of the polysulfides. The increased redox current of CP-TiC under a polarization of 0.8 V was in good accordance with the EIS results as well (Figure 2b).

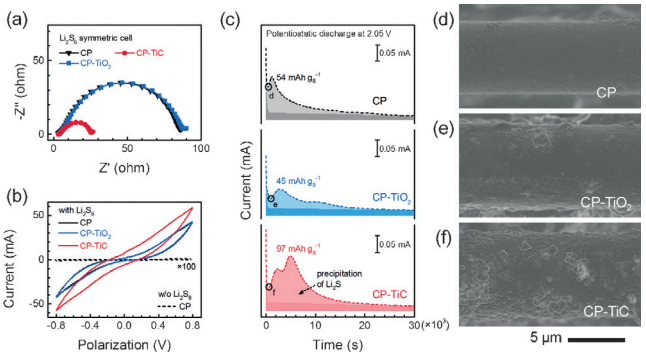

Figure 2. Electrochemical kinetics. a) EIS and b) CV of Li_2S_6 symmetric cells employing CP, CP-TiO_2, and CP-TiC as current collectors. c) Potentiostatic discharge curves of a Li_2S_8/tetraglyme solution at 2.05 V on different surfaces. The scale of the y-axis is indicated by the bar in the right. The lighter color indicates the precipitation of Li_2S, whereas the darker color represents the reduction of Li_2S_8/Li_2S_6. The capacity of Li_2S deposition is indicated over each curve. d–f) SEM images of the initial nucleation of Li_2S on different surfaces as indicated in (c). The scale bar is at the bottom right.

Except for the liquid–liquid transformation of the polysulfides, polar and conductive mediators also plays a crucial role at the liquid–solid boundary. It should be noted that theoretically three quarters of the capacity originates from the precipitation of Li_2S from Li_2S_4 precursors. Very recently, Chiang et al. showed the two-dimensional (2D) lateral growth of Li_2S on a carbon surface, which is initiated with nucleation under a certain overpotential.[25] The basic chemistry of classical crystal growth suggests that this growth mechanism can be further tuned by varying the surface energy between Li_2S and the substrates. Potentiostatic discharge curves of a Li_2S_8/tetraglyme solution at 2.05 V (ca. 0.1 V overpotential with respect to the equilibrium potential to drive the nucleation) were collected as shown in Figure 2c. Previously, all the cells were discharged to 2.06 V galvanostatically to consume most of the high-order polysulfides. The contributions of the progressive reduction of polysulfides (Li_2S_8/Li_2S_6) and the precipitation of Li_2S were mathematically modeled

and distinguished by dark and light colors, respectively (Supporting information, Figure S2). Obviously, CP-TiC had the highest activity towards Li_2S precipitation. Calculated from the integral of the current, the capacities of Li_2S precipitation on CP, CP-TiO_2, and CP-TiC were 109, 90, and 195 mAh g^{-1}, respectively, based on the weight of the sulfur in the catholyte. Additionally, since the precipitation of Li_2S is terminated by the impingement of insulating Li_2S islands on the surface, TiC can induce precipitation by promoting the growth of Li_2S along the radial direction. A similar effect was also enabled by an organic redox mediator.[26] However, inorganic compounds, which are more chemically stable, have not yet shown an analogous promotion. On the contrary, TiO_2 did not promote but rather poisoned the conductive carbon surface owing to its insulating nature.

The morphologies of the initial nucleation were further revealed by scanning electron microscopy (SEM). In Figure 2d, the CP surface was clean, with barely-observable Li_2S nuclei, owing to the poor affinity between polysulfides and carbon. A substantial energy barrier needs to be overcome for nucleation on CP. TiO_2 definitely increased the number of initial nucleation sites, probably owing to the smaller surface-energy difference between Li_2S and a polar surface than that between Li_2S and a non-polar carbon (Figure 2e). Nevertheless, the insulating TiO_2 inevitably inhibited the lateral growth of Li_2S once they came into contact, resulting in a low overall precipitation capacity. Only TiC, both polar and conductive, enabled a high abundance of nucleation sites and full surface coverage of Li_2S films (Figure 2f). Furthermore, the increased thickness of the coating layer on a single carbon fiber also suggested enhanced radial growth of Li_2S. Generally, the electrical conductivity plays a vital role in the electrochemical kinetics of sulfur redox by facilitating the reversible redox of solution-phase polysulfides on the electrode surface, promoting the further liquid–solid nucleation of Li_2S, and slowing down its impingement by perpendicular growth.

To translate the superior electrochemical kinetics into reality, nanosized TiC/mesoporous graphene (TiC@G) was synthesized through a confined carburization approach to serve as an advanced hybrid host material for the sulfur cathode. TiO_2@G hybrids were first obtained by hydrolysis of an impregnated tetrabutyl titanate precursor within the mesopores of graphene and subsequent mild dehydration at 400 °C. TiO_2 nanoparticles with an average size of circa 10 nm were obtained within the framework of mesoporous graphene (Figure 3a and Supporting Information, Figure S3). The small and uniform size was attributed to the confinement effect on the precursor (Supporting Information, Figure S4). Further carburization of TiO_2@G at 1600 °C under vacuum resulted in TiC@G hybrids, in which the TiC nanoparticles also exhibited a uniform distribution (Figure 3b) and were strongly immobilized on the graphene substrate (Figure 3c). During the entire synthetic procedure, the microstructure of mesoporous graphene was well retained (Supporting Information, Figure S5).

N_2 isotherms further confirmed that the desirable mesoporous structure of the graphene framework was preserved in the TiO_2@G and TiC@G hybrids (Figure 3d). TiO_2 and TiC nanoparticles were shown to be partially encapsulated in the mesopores, as the average size of the mesopores decreased slightly, which is in good accordance with the TEM images (Figure 3e). Nevertheless, the isotherms of TiO_2@G and TiC@G were quite similar, allowing a fair assessment of the electrochemical performance. The specific surface areas of graphene, TiO_2@G, and TiC@G were 2120, 1632, and 1611 $m^2 g^{-1}$, respectively. The nearly identical pore structures were attributed to the superior structural stability of the mesoporous graphene substrates[27] and the spatial confinement during carburization. Furthermore, the pore volume was still above 2.0 $cm^3 g^{-1}$, which was beneficial for buffering the volume fluctuation and transporting ions. X-ray diffraction (XRD) was used to characterize the crystal form of the hybrid materials (Figure 3f). TiO_2 was mainly amorphous owing to the low temperature of dehydration, whereas TiC exhibited its standard cubic structure (PDF 32-1383). The TiC@G hybrid combines the superb interfacial electrochemical kinetics of polar and conductive TiC and the inherently stable, porous, and conducting structure of mesoporous graphene.

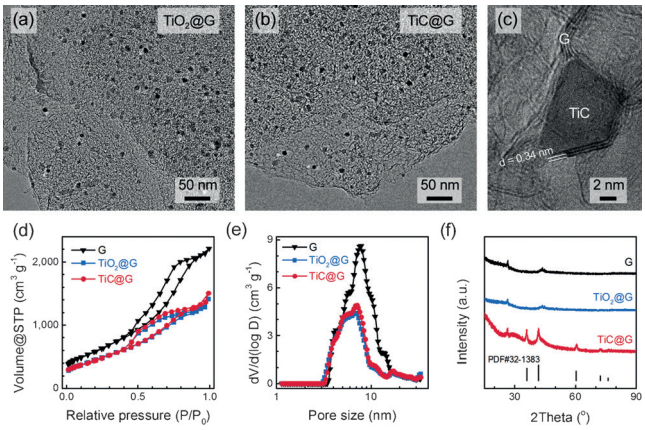

Figure 3. Structural characterization. Transition electron microscopy (TEM) images of a) TiO_2@G and b) TiC@G. High-resolution TEM image of c) TiC@G. d) N_2 isotherms and e) corresponding pore-size distribution based on density functional theory. f) XRD patterns.

Sulfur was thermally impregnated into each host using the routine melting-diffusion method at 155 °C, resulting in TiO_2@G/S and TiC@G/S composites with a sulfur content of 61 % (Supporting Information, Figure S6). The C/S composites served as cathodes without the assistance of any other conducting agent. To meet the demand for high energy density, a desirable areal sulfur loading of 3.5 mg cm^{-2} was controlled, which was comparable to that of the state-of-art Li–S batteries.[28]

In the cyclic voltammetry (CV) curves, the typical redox characteristics of sulfur are shown (Figure 4a). The two cathodic peaks at 2.2–2.4 V and 1.9–2.1 V corresponded to the reduction of elemental sulfur to soluble polysulfides and subsequent generation of solid Li_2S from the polysulfides, respectively. Some interesting attributes of TiC@G/S and TiO_2@G/S are summarized as follows: 1) The onset potentials for each redox peak were comparable, suggesting a similar capability of TiC and TiO_2 to adsorb reactive intermediates and to promote surface reactions; and 2) the peak potentials

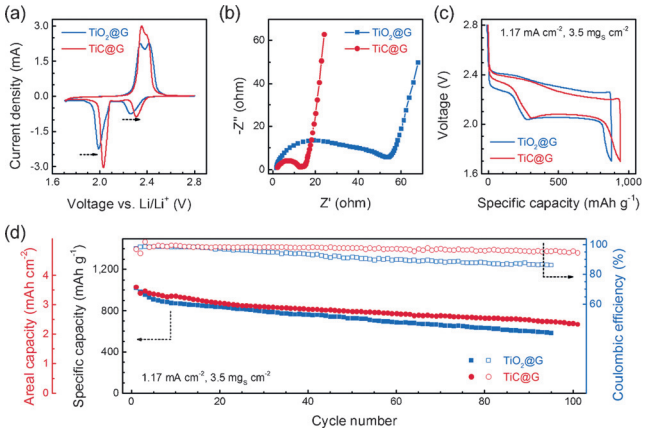

Figure 4. Electrochemical performance. a) Cyclic voltammograms; b) Nyquist plots at the fully charged state; c) galvanostatic discharge–charge profiles at a current density of 1.17 mAh cm^{-2} (0.2 C); and d) cycling performance at 0.2 C.

upshifted from TiO_2@G/S to TiC@G/S by 40–50 mV, indicating that electrochemical reactions proceed faster on the hybrid surface of TiC@G than on TiO_2@G. A higher negative potential was required to overcome the energy penalty of the extra diffusion process over the TiO_2@G interface.

EIS of TiC@G/S and TiO_2@G/S versus the lithium counter electrode also revealed the superb charge-transfer capability of TiC@G across the nanoscale liquid–solid interface (Figure 4b). The charge-transfer impedance of TiC@G/S was reduced by nearly four-fold that of TiO_2@G/S, further demonstrating the favorable electrochemical kinetics on TiC. TiO_2, although composited with a highly conductive graphene framework that satisfied the requirement for the macroscopic electron conduction, was incapable of directing the coupled adsorption-surface reaction process at the nanoscale interface. The electrochemical kinetics, which strongly depends on the demanding surface properties, could not be promoted. Therefore, desirable interfacial kinetics demands both surface polarity and intrinsic conductivity.

The typical multi-stage galvanostatic discharge–charge profiles of TiC@G/S and TiO_2@G/S at a current density of 1.17 mA cm^{-2} were compared in Figure 4c. The discharge capacities of TiC@G/S and TiO_2@G/S are 942 and 877 mAh g^{-1}, respectively. On one hand, the facilitated interconversion of polysulfides by TiC@G was indicated by the prolonged slope between the two plateaus. On the other hand, the conducting nature of TiC allowed the direct nucleation of Li_2S on TiC, creating more available nucleation sites. As a result, the TiC@G/S exhibited a longer lower-voltage plateau by successive growth of Li_2S from these nuclei. More importantly, the polarization and charging barriers of TiC@G/S were much lower than those of TiO_2@G/S, generating a remarkable energy efficiency of over 90%.

TiC@G/S also exhibited good cycling stability (Figure 4d). The initial capacity of TiC@G/S was 1032 mAh g^{-1}, corresponding to a desirable areal capacity of 3.6 mAh cm^{-2}. After 100 cycles, a capacity of 670 mAh g^{-1} was maintained with a Coulombic efficiency of over 95%. In contrast, TiO_2@G/S had a comparable initial capacity but displayed faster capacity fading and worse retention of Coulombic efficiency. A capacity of 580 mAh g^{-1} and Coulombic efficiency of 85% were obtained, suggesting the gradual deterioration of the TiO_2@G/S cathode and possible degradation of the lithium anode. The decay probably resulted from the low converting rate of surface-bound sulfur species on TiO_2, which, unfortunately, led to surface poisoning by unreacted polysulfides, prevented the subsequent adsorption, and weakened its suppression of polysulfide shuttle. The faster kinetics on TiC@G allows the full utilization of polysulfides within the cathode, with simultaneous suppression of the shuttle effect.

The stability of TiC@G/S was not extraordinarily high but comparable to many sulfur cathodes with high sulfur loadings over 3 mg cm^{-2}.[17,23] Note that the cathode was fabricated without engineering of other battery components such as the binder, separator, and current collector.[8,29] There are considerable opportunities to optimize the battery performance. However, the main effort here is to address the fundamental understanding of how the intrinsic conductivity of polar materials impacts the electrochemistry. We believe that this understanding will benefit the design of advanced sulfur-host materials.

In summary, we have shown the crucial role of the conductivity of the polar host in the electrochemical kinetics of Li–S batteries, which guided the advanced design of novel polar host materials for enhancing the performance of sulfur cathodes. Conductive TiC was shown to facilitate both the liquid–liquid transformation of polysulfides and liquid–solid nucleation/growth of Li_2S, whereas TiO_2 cannot. With this understanding, advanced polar hosts can be rationally designed, leading to high-performance Li–S batteries and other electrochemical devices using multi-electron chemistry.

Acknowledgements

This work was supported by the Natural Scientific Foundation of China (No. 21306103, 21422604, and 21561130151), Tsinghua University Initiative Scientific Research Program (No. 20161080166), and Grants from the Ministry of Science and Technology of the People's Republic of China (No. 2015CB932500 and 2016YFA0202500). We thank Chen-Zi Zhao and Chao Guan for preparing the digital micrographs of polysulfide adsorption.

Keywords: lithium–sulfur batteries · polysulfides · porous graphene frameworks · shuttle effect · titanium carbide

How to cite: *Angew. Chem. Int. Ed.* **2016**, *55*, 12990–12995
Angew. Chem. **2016**, *128*, 13184–13189

[1] a) P. G. Bruce, S. A. Freunberger, L. J. Hardwick, J.-M. Tarascon, *Nat. Mater.* **2012**, *11*, 19–29; b) A. Manthiram, S.-H. Chung, C. Zu, *Adv. Mater.* **2015**, *27*, 1980–2006.

[2] a) Y.-X. Yin, S. Xin, Y.-G. Guo, L.-J. Wan, *Angew. Chem. Int. Ed.* **2013**, *52*, 13186–13200; *Angew. Chem.* **2013**, *125*, 13426–13441; b) S. S. Zhang, *J. Power Sources* **2013**, *231*, 153–162; c) D.

Bresser, S. Passerini, B. Scrosati, *Chem. Commun.* **2013**, *49*, 10545 – 10562.
[3] a) X. Fang, H. Peng, *Small* **2015**, *11*, 1488 – 1511; b) J. Liang, Z.-H. Sun, F. Li, H.-M. Cheng, *Energy Storage Mater.* **2016**, *2*, 76 – 106.
[4] a) Q. Pang, X. Liang, C. Y. Kwok, L. F. Nazar, *J. Electrochem. Soc.* **2015**, *162*, A2567 – A2576; b) M. Liu, F. Ye, W. Li, H. Li, Y. Zhang, *Nano Res.* **2016**, *9*, 94 – 116.
[5] H.-J. Peng, Q. Zhang, *Angew. Chem. Int. Ed.* **2015**, *54*, 11018 – 11020; *Angew. Chem.* **2015**, *127*, 11170 – 11172.
[6] a) L. Ji, M. Rao, H. Zheng, L. Zhang, Y. Li, W. Duan, J. Guo, E. J. Cairns, Y. Zhang, *J. Am. Chem. Soc.* **2011**, *133*, 18522 – 18525; b) J. Song, T. Xu, M. L. Gordin, P. Zhu, D. Lv, Y.-B. Jiang, Y. Chen, Y. Duan, D. Wang, *Adv. Funct. Mater.* **2014**, *24*, 1243 – 1250; c) C.-P. Yang, Y.-X. Yin, H. Ye, K.-C. Jiang, J. Zhang, Y.-G. Guo, *ACS Appl. Mater. Interfaces* **2014**, *6*, 8789 – 8795; d) H.-J. Peng, T.-Z. Hou, Q. Zhang, J.-Q. Huang, X.-B. Cheng, M.-Q. Guo, Z. Yuan, L.-Y. He, F. Wei, *Adv. Mater. Interfaces* **2014**, *1*, 1400227; e) J. Song, M. L. Gordin, T. Xu, S. Chen, Z. Yu, H. Sohn, J. Lu, Y. Ren, Y. Duan, D. Wang, *Angew. Chem. Int. Ed.* **2015**, *54*, 4325 – 4329; *Angew. Chem.* **2015**, *127*, 4399 – 4403; f) G. Zhou, E. Paek, G. S. Hwang, A. Manthiram, *Nat. Commun.* **2015**, *6*, 7760.
[7] a) J. Guo, Z. Yang, Y. Yu, H. D. Abruna, L. A. Archer, *J. Am. Chem. Soc.* **2013**, *135*, 763 – 767; b) L. Ma, H. Zhuang, Y. Lu, S. S. Moganty, R. G. Hennig, L. A. Archer, *Adv. Energy Mater.* **2014**, *4*, 1400390; c) H. Chen, C. Wang, Y. Dai, S. Qiu, J. Yang, W. Lu, L. Chen, *Nano Lett.* **2015**, *15*, 5443 – 5448.
[8] Z. W. Seh, Q. Zhang, W. Li, G. Zheng, H. Yao, Y. Cui, *Chem. Sci.* **2013**, *4*, 3673 – 3677.
[9] a) Q. Pang, D. Kundu, M. Cuisinier, L. F. Nazar, *Nat. Commun.* **2014**, *5*, 4759; b) X. Tao, J. Wang, Z. Ying, Q. Cai, G. Zheng, Y. Gan, H. Huang, Y. Xia, C. Liang, W. Zhang, Y. Cui, *Nano Lett.* **2014**, *14*, 5288 – 5294.
[10] H. Yao, G. Zheng, P.-C. Hsu, D. Kong, J. J. Cha, W. Li, Z. W. Seh, M. T. McDowell, K. Yan, Z. Liang, V. K. Narasimhan, Y. Cui, *Nat. Commun.* **2014**, *5*, 3943.
[11] X. Liang, A. Garsuch, L. F. Nazar, *Angew. Chem. Int. Ed.* **2015**, *54*, 3907 – 3911; *Angew. Chem.* **2015**, *127*, 3979 – 3983.
[12] Z. Yuan, H.-J. Peng, T.-Z. Hou, J.-Q. Huang, C.-M. Chen, D.-W. Wang, X.-B. Cheng, F. Wei, Q. Zhang, *Nano Lett.* **2016**, *16*, 519 – 527.
[13] Z. W. Seh, J. H. Yu, W. Li, P.-C. Hsu, H. Wang, Y. Sun, H. Yao, Q. Zhang, Y. Cui, *Nat. Commun.* **2014**, *5*, 5017.
[14] a) Z. W. Seh, W. Li, J. J. Cha, G. Zheng, Y. Yang, M. T. McDowell, P.-C. Hsu, Y. Cui, *Nat. Commun.* **2013**, *4*, 1331; b) G. Zhou, Y. Zhao, C. Zu, A. Manthiram, *Nano Energy* **2015**, *12*, 240 – 249.
[15] J.-Y. Hwang, H. M. Kim, S.-K. Lee, J.-H. Lee, A. Abouimrane, M. A. Khaleel, I. Belharouak, A. Manthiram, Y.-K. Sun, *Adv. Energy Mater.* **2016**, *6*, 1501480.
[16] X. Liang, C. Hart, Q. Pang, A. Garsuch, T. Weiss, L. F. Nazar, *Nat. Commun.* **2015**, *6*, 5682.
[17] Z. Li, J. Zhang, X. W. Lou, *Angew. Chem. Int. Ed.* **2015**, *54*, 12886 – 12890; *Angew. Chem.* **2015**, *127*, 13078 – 13082.
[18] H. Wang, Q. Zhang, H. Yao, Z. Liang, H.-W. Lee, P.-C. Hsu, G. Zheng, Y. Cui, *Nano Lett.* **2014**, *14*, 7138 – 7144.
[19] S. S. Zhang, D. T. Tran, *J. Mater. Chem. A* **2016**, *4*, 4371 – 4374.
[20] S. Rehman, S. Guo, Y. Hou, *Adv. Mater.* **2016**, *28*, 3167 – 3172.
[21] Y. Zhang, Y. Zhao, A. Yermukhambetova, Z. Bakenov, P. Chen, *J. Mater. Chem. A* **2013**, *1*, 295 – 301.
[22] X. Tao, J. Wang, C. Liu, H. Wang, H. Yao, G. Zheng, Z. W. Seh, Q. Cai, W. Li, G. Zhou, C. Zu, Y. Cui, *Nat. Commun.* **2016**, *7*, 11203.
[23] J. Zhang, H. Hu, Z. Li, X. W. Lou, *Angew. Chem. Int. Ed.* **2016**, *55*, 3982 – 3986; *Angew. Chem.* **2016**, *128*, 4050 – 4054.
[24] M. Yu, J. Ma, H. Song, A. Wang, F. Tian, Y. Wang, H. Qiu, R. Wang, *Energy Environ. Sci.* **2016**, *9*, 1495 – 1503.
[25] F. Y. Fan, W. C. Carter, Y.-M. Chiang, *Adv. Mater.* **2015**, *27*, 5203 – 5209.
[26] L. C. H. Gerber, P. D. Frischmann, F. Y. Fan, S. E. Doris, X. Qu, A. M. Scheuermann, K. Persson, Y.-M. Chiang, B. A. Helms, *Nano Lett.* **2016**, *16*, 549 – 554.
[27] J. L. Shi, H. F. Wang, X. L. Zhu, C. M. Chen, X. Huang, X. D. Zhang, B. Q. Li, C. Tang, Q. Zhang, *Carbon* **2016**, *103*, 36 – 44.
[28] M. Hagen, D. Hanselmann, K. Ahlbrecht, R. Maca, D. Gerber, J. Tubke, *Adv. Energy Mater.* **2015**, *5*, 1401986.
[29] a) R. Fang, S. Zhao, P. Hou, M. Cheng, S. Wang, H.-M. Cheng, C. Liu, F. Li, *Adv. Mater.* **2016**, *28*, 3374 – 3382; b) H. Wang, W. Zhang, H. Liu, Z. Guo, *Angew. Chem. Int. Ed.* **2016**, *55*, 3992 – 3996; *Angew. Chem.* **2016**, *128*, 4060 – 4064; c) S. Chen, F. Dai, M. L. Gordin, Z. Yu, Y. Gao, J. Song, D. Wang, *Angew. Chem. Int. Ed.* **2016**, *55*, 4231 – 4235; *Angew. Chem.* **2016**, *128*, 4303 – 4307.

Received: June 12, 2016
Published online: August 11, 2016

